Available online at www.sciencedirect.com
ScienceDirect
Proceedings of the Combustion Institute 31 (2007) 3285–3292
Proceedings of the Combustion Institute
www.elsevier.com/locate/proci

Experimental study of spinning combustion in a mesoscale divergent channel

Bo Xu *, Yiguang Ju

Department of Mechanical and Aerospace Engineering, Princeton University, Princeton, NJ 08544, USA

Abstract

Quasi-steady and unsteady propagations of methane and propane–air premixed flames in a mesoscale divergent channel were investigated experimentally and theoretically. The emphasis was the impact of variable cross-section area and the flame-wall coupling on the flame transition between different regimes and the onset of flame instability. Experimentally, for the first time, spinning flames were observed in mesoscale combustion for both lean and rich methane and propane–air mixtures in a broad range of equivalence ratios. The spinning flames rotated in either clockwise or counterclockwise direction with equal probability. The results showed that for a fixed equivalence ratio, there was a critical flow rate, above which flame starts to spin. The spin frequency was approximately proportional to the flame speed. It was also found that the spinning flame only occurred after the transition from fast flame regime to slow flame regime. The flame propagation speed and the effective Lewis number were obtained analytically. Experimental observation and theoretical analysis suggested that regardless of the magnitude of mixture Lewis numbers, the flame-wall coupling will significantly increase the effective Lewis number and lead to a new mechanism to promote the thermal diffusion instability.

Keywords: Mesoscale; Microscale; Flame instability; Premixed flame; Spin flame

1. Introduction

In mesoscale combustion (combustor length scale ~ flame quenching diameter), the increase of surface to volume ratio increases the wall heat loss and can lead to flame extinction [1–6]. On the other hand, the reduction of thermal inertia significantly reduces the response time of the wall and leads to strong flame-wall coupling and extension of burning limits [7–12]. This flame-wall coupling dramatically changes the nature of flame propagation and yields multiple flame regimes [11,13,14]. Recent study [14] showed that the transition of flame regimes is dramatically affected by the channel width and the flow velocity. In fact, all practical combustors have variable channel width. As a result, the simultaneous changes of channel width and flow rate will significantly modify the heat loss and flame-wall coupling. Therefore, it is of great interest to understand how the variation of channel width will affect the flame propagation and transition. Unfortunately, most of the studies in mesoscale combustion only focused on flame propagation in a channel with a constant area.

In addition to quasi-steady propagation, flame instability is also very important for combustion control. The instability of combustion waves has been extensively studied. In gaseous combustion, there are basically two intrinsic instability mechanisms: the hydrodynamic instability [15,16] and

* Corresponding author. Fax: +1 609 258 6233.
E-mail address: bxu@princeton.edu (B. Xu).

1540-7489/$ - see front matter © 2006 Published by Elsevier Inc. on behalf of The Combustion Institute.
doi:10.1016/j.proci.2006.07.241

Nomenclature

C	Ratio of the heat capacity of gas phase to solid phase: $\rho_g C_p A_g/\rho_w C_w A_w$
C_p, C_w	Gas phase specific heat at constant pressure, and wall heat capacity
D	Differential operator, d/dx
E	Activation energy
h	Heat transfer coefficient on wall surface
$H(\xi_f)$	Normalized rate of heat transfer on the inner wall surface, $4Nu/\mathrm{d}^2(\xi_f)$
j	$\alpha_w/\alpha_g C$.
Le	Lewis number
m	Normalized flame speed, $U(\xi_f) - U_f$
m_v	Normalized volumetric flow rate, $\overline{m}_v/(U_{\mathrm{ad}}\delta_f^2)$
p	$-U_f/C$
Q	Volumetric flow rate in cm^3/s.
R_0	Universal gas constant
u	Dimensional flow velocity
U_{ad}	Dimensional adiabatic flame speed
$U(\xi_f)$	Normalized flow velocity, $m_v/\pi\mathrm{d}^2(\xi_f)/4$
U_f	Normalized flame propagation velocity, u_f/U_{ad}
Y	Normalized fuel concentration, $Y_F/Y_{F\infty}$
α	$T/(T_{\mathrm{ad}} - T_{-\infty})$
α_g, α_w	Thermal diffusivity
β	Zeldovich number, $E(T_{\mathrm{ad}} - T_\infty)/R_0 T_{\mathrm{ad}}^2$
ξ	Streamwise coordinate normalized by $\lambda/\rho C_p U_{\mathrm{ad}}$
θ	Normalized temperature, $(T - T_\infty)/(T_{\mathrm{ad}} - T_\infty)$
λ	Thermal conductivity or eigenvalues (see Eq. (5))
δ_f	Flame thickness, α_g/U_{ad}

Subscripts

ad	Adiabatic parameters
f	Parameters at flame fronts
g	Gas phase
w	Wall
∞	Parameters of unburned mixture at infinity

the diffusive-thermal instability [17–19]. In mesoscale combustion, since the long wavelength hydrodynamic instability is suppressed, the thermal diffusion instability plays a dominant role. The linear stability analysis [18,19] showed that thermal diffusion instability results in cellular flames when the Lewis number (Le) is less than a critical value less than unity and pulsating/traveling flames when Le is larger than a critical value, i.e., $Le^* = \beta(Le - 1) > 10.9$, where β is the Zeldovich number [19]. For non-adiabatic flames, Joulin and Clavin [19] showed that heat loss can significantly reduce the critical value and render the pulsating instability to occur at a smaller Le. For near-limit flames, Booty et al. [20] showed that Le^* for traveling instability can be as small as 3.6. Experimentally, low Lewis number cellular instability has been studied by using the downward propagating flames [21–23] and the burner stabilized polyhedral flames [24–28]. Spinning flames in a sudden expansion tube caused by heat loss and preferential diffusion were also reported for methane/air and propane/air flames [28], which were similar as the rotating polyhedral butane–air flames observed by Sohrab and Law [26]. Pulsating flames have been observed in porous plug [29], downward propagating sooting flames [30], lean butane–air flames [31], and in solid combustion [32,33]. Most of these studies focused on heat loss. Studies [34,35] also showed that the traveling instability existed for near unity Lewis number mixtures when radiation resulted in multiple flame regimes. For mesoscale combustion, flame-wall coupling also results in multiple flame regimes. Therefore, this bifurcation may also trigger the flame instability for mixtures even with Le near unity. Unfortunately, the existence of traveling instability due to wall-flame coupling in mesoscale combustion has not been observed. Although some previous studies reported that flame instability occurred near the inlet of mesoscale channels [13,28,36,37], this instability was either purely a repeating cycle of re-ignition and quenching or a result of heat loss effect to the burner and not caused by the intrinsic thermal diffusion instability.

The goal of this study is to investigate experimentally and theoretically the flame transition between different regimes and the traveling instability in a divergent mesoscale channel using CH_4 and C_3H_8–air mixtures.

2. Theoretical analysis

In view of the difficulty in numerical simulation for flame bifurcations, an analysis was performed to understand qualitatively the general dynamics of flame propagation in a divergent channel. To simplify the problem, we first introduced the one-dimensional quasi-steady state assumption. The validity of quasi-steady state assumption will be confirmed later using unsteady numerical simulation. A more detailed description of the theoretical analysis can be found in [11]. By neglecting the external heat loss and further

assuming a small divergent angle, the normalized energy conservation equations of the gas and the wall and the species conservation equation become

$$\begin{aligned} m(\xi_f)\frac{d\theta}{d\xi} &= \frac{d^2\theta}{d\xi^2} - H(\xi_f)(\theta-\theta_w) \\ &\quad + \exp(\beta(\theta_f-1)/2)\delta(\xi-\xi_f) \\ m(\xi_f)\frac{dY}{d\xi} &= \frac{1}{Le}\frac{d^2Y}{d\xi^2} - \exp(\beta(\theta_f-1)/2)\delta(\xi-\xi_f) \\ -U_f\frac{d\theta_w}{d\xi} &= \frac{d^2\theta_w}{d\xi^2}\frac{\alpha_w}{\alpha_g} + H(\xi_f)C(\theta-\theta_w). \end{aligned} \tag{1}$$

The boundary conditions for infinite long channels are given below

$$\begin{aligned} &\xi\to-\infty, \quad \theta=\theta_w=0, \quad Y=1; \\ &\xi\to+\infty, \quad \frac{d\theta}{d\xi}=\frac{d\theta_w}{d\xi}=0, \quad Y=0. \end{aligned} \tag{2}$$

As opposed to the analysis in [11], here the flame propagation speed is a function of flame location ξ_f. The temperature equation can be rewritten as

$$\begin{aligned} &[jD^3-(jm+p)D^2+(-jH-H+mp)D+pH \\ &\quad +mH]\theta=0. \end{aligned} \tag{3}$$

The solution of Eq. (3) is straight forward. Due to the limit of space, we only show the solution of flame speed

$$m=e^{\beta(\theta_f-1)/2}, \quad \theta_f=F[m,j,p,H]. \tag{4}$$

Detailed algebraic form for F is similar to that in [11] except that the flow velocity here is not constant. When the wall thermal diffusivity is small compared to that of the gas phase (e.g., quartz tube), the solution in Eq. (4) reduces to

$$\begin{aligned} \ln m^2 &= -\frac{\beta}{2}\Big\{(m+2p)\sqrt{(H+mp)^2+4Hp^2}+(mH+2mp^2+m^2p) \\ &\quad \Big/(m+p)\sqrt{(H+mp)^2+4Hp^2}\Big\}. \end{aligned} \tag{5}$$

In the limit of zero thermal conductivity of the wall ($j=0$) and zero flow speed (i.e., $p=mC$), there is heat transfer between the flame and the wall but not inside the wall. Equation (5) reduces to the solution of a diluted particle laden flame [19],

$$\ln m^2 = -\frac{\beta H(2m^2+CH)}{(m^2+CH)^2}. \tag{6}$$

And in the limit of $C\to 0$, the wall temperature barely changes and there is no flame-wall coupling, Eq. (5) reduces to

$$\ln m^2 = -\frac{2\beta H}{m^2}. \tag{7}$$

Equations (4) and (5) represent the flame speed with flame-wall coupling and Eq. (7) is merely the flame propagation speed in a cold channel without flame-wall coupling. Equations (4), (5), and (7) will be used to estimate the flame speed and the effective Lewis number.

3. Experimental setup

The experiment of mesoscale flame propagation in a variable cross-section area channel was examined by using a divergent quartz tube. The experimental setup is schematically shown in Fig. 1. The tube (Fig. 1b) is vertically mounted and has two constant-area Sections 1 and 4, a converging Section 2, and a diverging Section 3, if seen from the inlet. The inner diameter is 10 mm in the constant-area sections and is 4 mm at the throat. The wall thickness is 1 mm. The lengths of the diverging and converging parts are 50 mm. Section 1 is 600 mm in length ($L/d>60$) to ensure a fully developed flow before entering Section 2. The convergent and divergent angles are all 6.9°. A mesh grid is placed near the inlet of the tube to eliminate any flow disturbance. The divergent cross-section will ensure that the final stabilization flame is always in the slow flame regime with a strong flame-wall coupling. The flow rates control system of fuel and air consists of a LabView-controlled A/D board (DAQ NI PCI-6014) and two mass flow controllers (Brooks 5850E). To ensure sufficient mixing, a mixing cylinder with the volume 150 cm^3 is used upstream. In addition, a flash arrester is used between the mixing cylinder and the quartz tube. The flame propagation history was recorded by a high-speed camera (PHOTRON) at 500 frames per second.

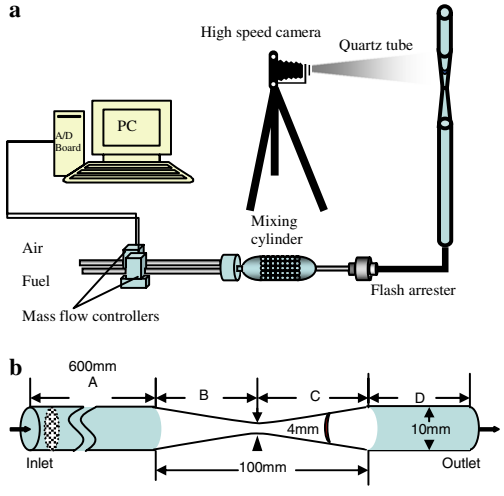

Fig. 1. Schematic of the experimental setup.

4. Numerical simulation

To quantitatively examine the flame-wall coupling and validate the theory, we also seek numerical simulations of unsteady and quasi-steady flame propagation in the diverging quartz tube with detailed transport properties and chemical kinetics. Although in most cases flame is not one-dimensional, in order to understand the essence and avoid the excessive computation cost [14], we also adopted the one-dimensional model. For chemical kinetics, GRI3.0 [38] was employed and the transport properties were computed using Chemkin [39] database. The governing equations for gas and solid phases can be found in [11]. In the simulation, the parameters of the quartz tube are the same as in the experiment and analysis. The Nusselt number of inner wall surface is 4.36. Heat transfer through the outside wall is natural convection. The radiation emissivity of the outer surface of the quartz wall is 0.93; the density, heat capacity, and heat conductivity of the wall are set as 2,650 kg/m^3, 750 J/kg/K, and 2 W/m/K, respectively.

5. Results and discussion

In the experiments, four different flame modes, the propagating flame, a self-extinguished flame, the stabilized planar flame, the spinning flame, were observed. For a given equivalence ratio, when the mixture is ignited at the tube exit, a propagating flame is formed in Section 4 and propagates into Section 3. Figure 2 shows the trajectory history of transitions from a propagating flame to either a stabilized planar flame at $\phi = 1.5$ and $Q = 3$ cm^3/s (a) or a spinning flame at $\phi = 1.5$ and $Q = 5$ cm^3/s (b). As shown in Fig. 2a, flame propagation has three stages. First, as the flame propagates in the constant area section, the flame speed is almost constant. Second, as the flame enters the convergent section, the decrease of tube diameter resulted in an increase of the local flow velocity and thus a decrease of flame propagation speed. Third, as the flame further moves upstream, it is stabilized in the convergent section around $t = 500$ ms. At a larger flow rate (Fig. 2b), the propagating flame slows down to almost zero propagation speed first in the convergent section and then transforms to a spinning flame around $t = 400$ ms. Both the spin location and the frequency will not change. This transition process occurs when the flame propagation speed approaches zero, which indicates that the onset of flame spin requires flame-wall coupling. It was also found that the transitions between spinning flames and stabilized planar flames can be induced by controlling the flame-wall coupling externally (i.e., by cooling or heating up the wall). This observation further confirmed that the flame

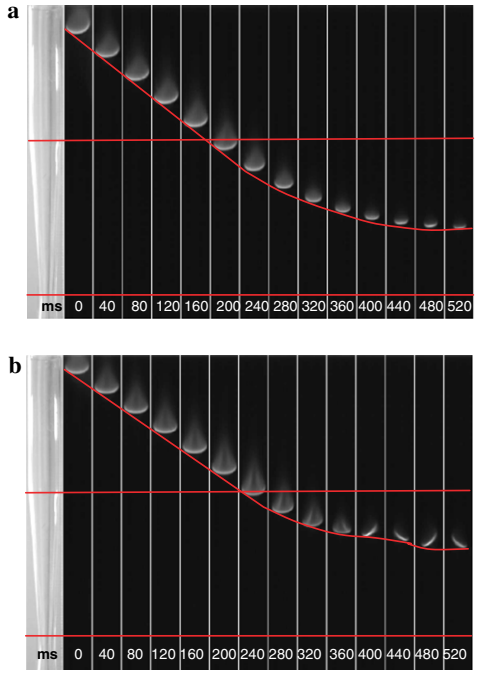

Fig. 2. Trajectory history for C_3H_8–air flames. (a) $\phi = 1.5$, $Q = 3$ cm^3/s; (b) $\phi = 1.5$, $Q = 5$ cm^3/s.

instability is controlled by flame-wall thermal coupling. In addition, spinning flames were observed for both methane and propane flames at lean and rich conditions and the spin direction was randomly selected with equal probability. The random selection of spinning direction implies that the instability is not governed by flow motion but by the diffusion process. Furthermore, the spinning flame was also confirmed in another tube with only one divergent section and observed when the tube was set horizontal or upside down. Therefore, it can be concluded that this spinning flame is not produced by buoyancy and is governed by the flame-wall thermal coupling.

When the flow rate is decreased, the propagating flame will transform to a stabilized planar flame at a smaller diameter where the flow velocity balances with the flame speed. If the flow rate is further reduced, the propagating flame will either extinguish at a smaller tube diameter or pass through the throat.

Figure 3 shows the different regimes for self-extinguished flames, stabilized planar flames, and spinning flames. It is seen that for both methane–air flames (a) and propane–air (b) there is a critical flow rate, above which spinning flame exists and below which flame is stable. For methane flames, there is a quenching limit at low flow rates. For propane flames, the quenching limit exists for lean and rich mixtures at low flow rates. At near stoichiometric conditions and low flow

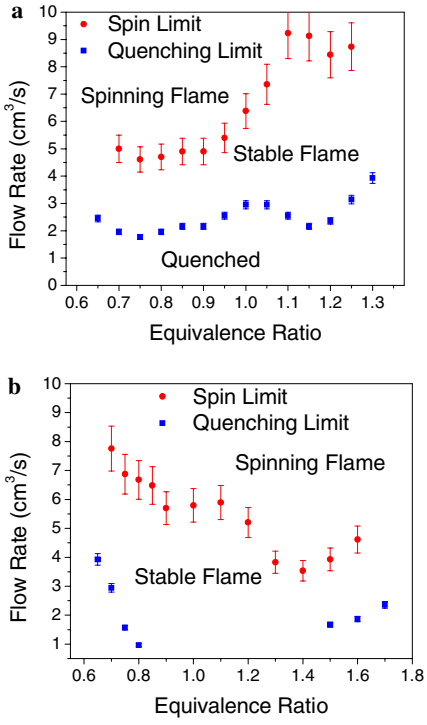

Fig. 3. Critical flow limits at different equivalence ratio. (a) Methane; (b) propane.

rates, propane flames will pass the throat area without extinction.

Depending on *Le*, two different spinning flame shapes, an "*L*" shaped flame (flame tail is open) and an "*S*" shaped flame (flame tail closed), were observed for both methane and propane flames. Figure 4 shows the flame shapes of rich ($Le < 1$) and lean ($Le > 1$) propane spinning flames at $\phi = 1.6$ and 0.8, respectively, and the corresponding time sequences in one cycle are shown in Fig. 5. The open tail (Fig. 5a) occurs at $Le < 1$ (rich case) because the insufficient reactant is the lighter molecule (oxygen). Figure 5 also shows that the flame spinning velocity for the lean propane flame is much faster than that of the rich case.

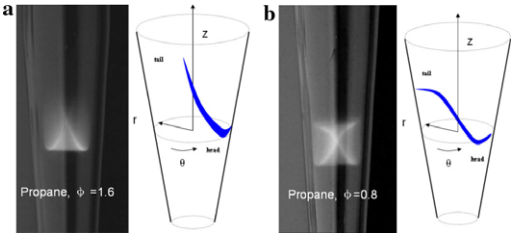

Fig. 4. Structures of lean and rich propane spin flames.

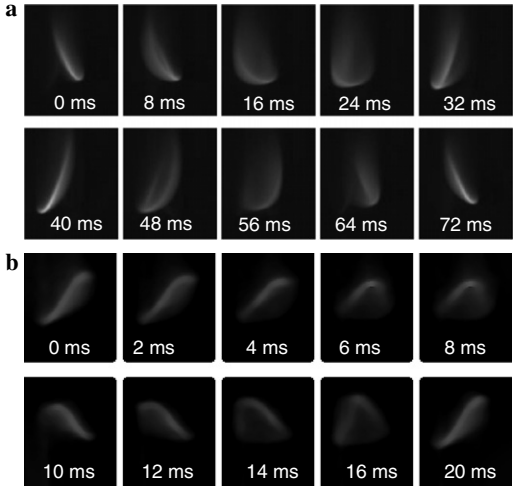

Fig. 5. Time sequences of spin flames in one period for C_3H_8–air mixtures. (a) $\phi = 1.6$, $Q = 8.84$ cm^3/s, $Le < 1$; (b) $\phi = 0.8$, $Q = 6.9$ cm^3/s, $Le > 1$.

The spinning frequencies of methane and propane flames at different equivalence ratios and flow rates are shown in Fig. 6. The error bar shown here is the frequency fluctuation caused by environment perturbation, i.e., room temperature change, not from the measurement. The average flame speeds S_a estimated at a smaller

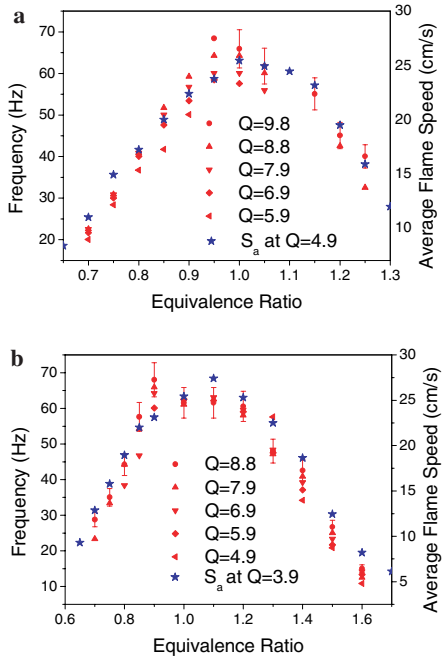

Fig. 6. Frequencies of methane and propane spin flames at different equivalence ratio. The flow rate Q is in cm^3/s. (a) Methane; (b) propane.

flow rate is also plotted. A smaller flow rate is used for S_a because the flame is less curved. It is seen that the spin frequency is roughly proportional to the average flame speed and only slightly affected by the flow rate.

The dependence of spinning frequency on the flow rate history of methane flames at $\phi = 1.05$ is shown in Fig. 7. Zero frequency represents a stabilized planar flame. When the flow rate decreases from 10 cm^3/s, the flame spins at almost constant frequency until point A; when the flow rate increases from 3 cm^3/s, it remains as a planar stable flame until point B. That is, there exists a bifurcation region between A and B where stabilized planar flame and spin flame coexist. This hysteresis phenomenon reflects the thermal historic effect of the wall and further indicates that the wall temperature for flame-wall coupling is the key parameter.

Experimental observation showed that the spinning flame always occurred after the flame transition from the fast flame to the slow flame. The flame regime diagram calculated from the theoretical result (Eq. (4)) clearly shows the dependence of flame speed on the tube diameter at different flow rates and is plotted in Fig. 8. It is seen that at zero flow rates, there is only one flame branch. When the flow rate is not zero, a slow flame branch emerges beyond the extinction limit and the flame transition from the fast flame branch to the slow flame branch occurs as the flame propagates into the divergent tube. The transition could be either direction transition or extinction transition depending on the flow rate. The spinning flame always occurs after the transition from fast flame branch to slow flame branch.

To validate the theoretical analysis, the diagram of unsteady and quasi-steady flame transition computed for methane–air mixture at $\phi = 1$ using the detailed chemistry is shown in Fig. 9.

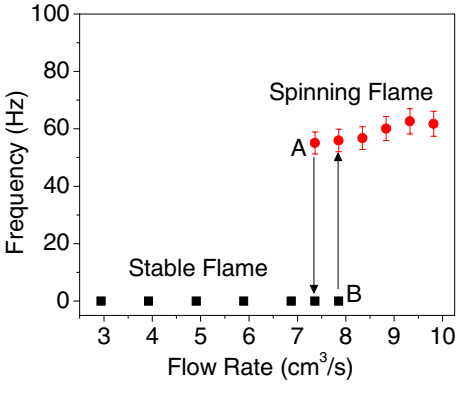

Fig. 7. Spin frequency at different flow rates for CH_4–air flame with $\phi = 1.05$.

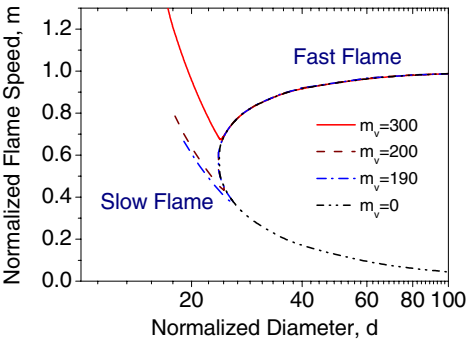

Fig. 8. Flame transition diagram at different diameters from theoretical analysis.

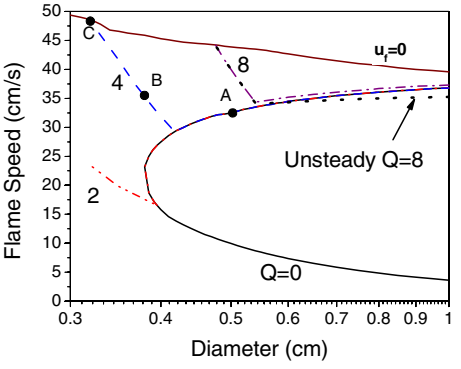

Fig. 9. Flame transition diagram at different diameters from one-dimensional simulation of methane flames with detailed chemistry ($\phi = 1$).

The dot line is the unsteady calculation at $Q = 8$ cm^3/s and all the other lines are quasi steady state calculations. It is seen that when the quasi-steady state assumption was employed, similar diagram to the theoretical analysis was obtained. There is a transition from a fast flame branch to a slow flame branch at nonzero flow rates. For example, at $Q = 4$ cm^3/s, the flame follows branch A, and then transfers to branch B and finally reaches point C, where the propagation speed reduces to zero and a steady state is reached. This transition occurs at a smaller diameter for a lower flow rate. At $Q = 8$ cm^3/s, an unsteady planar flame propagating into a divergent tube was also simulated (dot line) and the result agrees fairly well with the quasi-steady state curve (dash dot line). As such, the quasi-steady state approximation is reasonable to model the flame transition in a divergent channel.

Since, the instability is governed by the thermal diffusion process in gas and solid phases, the estimation of an effective Lewis number is important to understand the mechanism of the spinning flames. Thermal coupling with the wall can raise

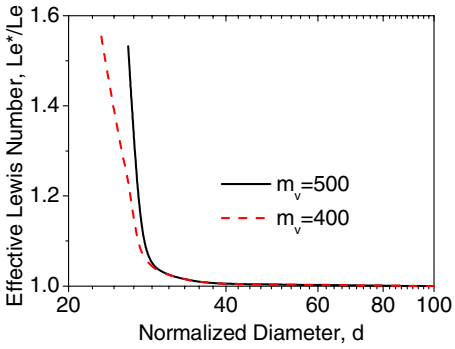

Fig. 10. Effective Lewis number from theoretical analysis.

the effective Lewis number of the problem so that instabilities can be observed even when the Lewis number of the gas-phase is far below the critical value. The effective Lewis number can be simply extracted from the theoretical results by matching the flame speed in Eq. (4) or (5) with that in Eq. (7) using an increased thermal diffusivity. The calculated effective Lewis number is shown in Fig. 10. It is seen that the effective Lewis number increases as the diameter decreases. In particular, when the flame starts to couple with the wall, the effective Lewis number increases dramatically. In addition, the increase of flow rate results in an increase of the effective Lewis number at the same tube diameter. For methane–air flames that have Lewis number around unity, the effective Lewis number with flame-wall coupling can be as high as 1.5. If the Zeldovich number β is around 10, the reduced Lewis number $\beta(Le-1)$ will be larger than the critical value for traveling flames ($Le^* = 3.6$) [20]. This explains why the flow rate is important to cause the onset of the traveling flame. Although the real spinning flame is three-dimensional (3D), the flame spinning is controlled by the leading flame head close to the hot wall and the frequency is roughly proportional to the flame speed of the flame head. Of course, a quantitative prediction of flame spinning needs three-dimensional unsteady computation with detailed chemistry. Therefore, it can be concluded that the spinning flame observed in this experiment at near unity Lewis numbers is not directly caused by heat loss but by heat gain through the flame-wall coupling and that the critical Lewis number may still be applicable if the effective Lewis number from the flame-wall coupling is employed.

6. Conclusions

Laminar premixed flame propagation in a mesoscale diverging quartz tube was studied and four different propagation waves were observed: a stabilized planar flame, a self-extinguished flame, a propagating flame and a spinning flame. Methane–air and propane–air flames at large range of equivalence ratios and flow rates were examined and the results showed that the spin flame exists for both lean and rich methane–air or propane–air mixtures. The spin wave is caused by the flame bifurcation and the strong thermal coupling between the flame and the wall and occurs at a broad range of Lewis numbers. Flame diagram and the effective Lewis number are theoretically predicted. The onset of spinning flame is explained by using an effective Lewis number. The spin direction is randomly selected during the initiation of the spin flame and remains unchanged afterwards. The critical flow rate when the flame starts to spin highly depends on the equivalence ratio. The spin frequency is roughly proportional to the flame speed.

Acknowledgment

This research is partly supported by National Science Foundation CST-0418403.

References

[1] A.C. Fernandez-Pello, *Proc. Combust. Inst.* 29 (2002) 883–899.
[2] J. Vican, B.F. Gajdeczko, F.L. Dryer, D.L. Milius, I.A. Aksay, R.A. Yetter, *Proc. Combust. Inst.* 29 (2002) 909–916.
[3] L. Sitzki, K. Borer, E. Schuster, P.D. Ronney, S. Wussow, in: Proceedings of the Third Asia-Pacific Conference on Combustion, Seoul, 2001, p. 473.
[4] D.B. Spalding, *Proc. R. Soc. Lond. A* 240 (1220) (1957) 83–100.
[5] B. Lewis, G.V. Elbe, *Combustion, Flame and Explosion of Gases*, Academic Press, NY, 1967, p. 261.
[6] J. Daou, J. Dold, M. Matalon, *Combust. Theory Model.* 6 (2002) 141–153.
[7] F.J. Weinberg, *Nature* (1971) 233–239.
[8] Y. Ju, S. Minaev, *Proc. Combust. Inst.* 29 (2002) 949–956.
[9] P.D. Ronney, *Combust. Flame* 135 (2003) 421–439.
[10] Y. Ju, W. Choi, *Combust. Flame* 133 (2003) 483–493.
[11] Y. Ju, B. Xu, *Proc. Combust. Inst.* 30 (2005) 2445–2453.
[12] T.T. Leach, C.P. Cadou, *Proc. Combust. Inst.* 30 (2005) 2437–2444.
[13] K. Maruta, T. Katoka, N.I. Kim, S. Minaev, R. Fursenko, *Proc. Combust. Inst.* 30 (2005) 2429–2436.
[14] Y. Ju, B. Xu, *Combust. Sci. Technol.* 178 (2006) 1723–1753.
[15] L. Landau, *Acta Physicochim. (URSS)* 19 (1944) 77.
[16] G. Darrieus, *Propagation d'un front de flamme. Essai de Theorie des vitesses arnoles de Deflagration par developpment spontanne de la Turbulence*. Sixth

International Congress of Applied Mathematics, 1946.
[17] G.I. Barenblatt, Y.B. Zeldovich, A.G. Istratov, *J. Appl. Mech. Technol. Phys.* 4 (1962) 21–26.
[18] G.I. Sivashinsky, *Combust. Sci. Technol.* 15 (3–4) (1977) 137–146.
[19] G. Joulin, P. Clavin, *Combust. Flame* 35 (2) (1979) 139–153.
[20] M.R. Booty, S.B. Margolis, B.J. Matkowsky, *SIAM J. Appl. Math.* 47 (6) (1987) 1241–1286.
[21] G.H. Markstein, *Nonsteady Flame Propagation*, Pergamon, New York, 1964.
[22] T. Mitani, F.A. Williams, *Combust. Flame* 39 (1980) 169–190.
[23] P.D. Ronney, *Combust. Flame* 82 (1990) 1–14.
[24] S. Smithels, K. Ingle, *J. Chem. Soc.* 61 (1892) 204.
[25] S. Ishizuka, C. K. Law, in: Proceedings of the Nineteenth Symp., 1982, p. 327.
[26] S.H. Sohrab, C.K. Law, *Combust. Flame* 62 (1985) 243–254.
[27] L.J. Rosen, R.L. Axelbaum, *Combust. Flame* 126 (2001) 1433–1444.
[28] M.J. Kwon, B.J. Lee, S.H. Chung, *Combust. Flame* 105 (1996) 180–188.
[29] M. el-Hamdi, M. Gorman, K.A. Robbins, *Combust. Sci. Technol.* 94 (1993) 87–101.
[30] I.M. Gololobov, E.A. Granovskii, Yu.A. Gostintsev, *Combust. Expl. Shock Waves* 17 (1981) 22–26.
[31] H.G. Pearlman, P.D. Ronney, *Phys. Fluids* 6 (12) (1994) 4009–4018.
[32] A.G. Merzhanov, A.K. Filonenko, I.P. Borovinskaya, *Phys. Chem. Soc.* 208 (1973) 122–125.
[33] Y.M. Maksimov, A.T. Pak, G.V. Lavrenchuk, Yu. S. Naiborodenko, A.G. Merzhanov, *Combust. Expl. Shock Waves* 15 (1979) 415–418.
[34] K. Maruta, Y. Ju, A. Honda, T. Niioka, *Proc. Combust. Inst.* 27 (1998) 2611–2617.
[35] Y. Ju, C.K. Law, K. Maruta, T. Niioka, *Proc. Combust. Inst.* 28 (2000) 1891–1900.
[36] F. Richecoeur, D.C. Kyritsis, *Proc. Combust. Inst.* 30 (2005) 2419–2427.
[37] D.G. Norton, D.G. Vlachos, *Chem. Eng. Sci.* 58 (2003) 4871–4882.
[38] G.P. Smith, D.M. Golden, M. Frenklach, N.W. Moriarty, B. Eiteneer, M. Goldenberg, C.T. Bowman, R.K. Hanson, S. Song, W.C. Gardiner, Jr., V.V. Lissianski, Zh. Qin, available at http://www.me.berkeley. edu/gri_mech/.
[39] R.J. Kee, J.F. Grcar, M.D. Smooke, J.A. Miller, Report No. SAND85-8240, Sandia National Laboratories, 1985.